Carbohydrate Polymers 121 (2015) 155–162

Contents lists available at ScienceDirect

Carbohydrate Polymers

journal homepage: www.elsevier.com/locate/carbpol

Mechanical, barrier and morphological properties of starch nanocrystals-reinforced pea starch films

Xiaojing Li, Chao Qiu, Na Ji, Cuixia Sun, Liu Xiong, Qingjie Sun*

School of Food Science and Engineering, Qingdao Agricultural University, Qingdao, Shandong Province 266109, China

ARTICLE INFO

Article history:
Received 12 July 2014
Received in revised form 6 December 2014
Accepted 8 December 2014
Available online 31 December 2014

Keywords:
Starch
Nanocrystal
Films
Tensile strength
Water vapor permeability
Thermal stability

ABSTRACT

To characterize the pea starch films reinforced with waxy maize starch nanocrystals, the mechanical, water vapor barrier and morphological properties of the composite films were investigated. The addition of starch nanocrystals increased the tensile strength of the composite films, and the value of tensile strength of the composite films was highest when starch nanocrystals content was 5% (w/w). The moisture content (%), water vapor permeability, and water-vapor transmission rate of the composite films significantly decreased as starch nanocrystals content increased. When their starch nanocrystals content was 1–5%, the starch nanocrystals dispersed homogeneously in the composite films, resulting in a relatively smooth and compact film surface and better thermal stability. However, when starch nanocrystals content was more than 7%, the starch nanocrystals began to aggregate, which resulted in the surface of the composite films developing a longitudinal fibrous structure.

1. Introduction

A large amount of contemporary research seeks environmentally friendly material to prevent the pollution that petroleum-based plastic waste produces (Famá, Goyanes, & Gerschenson, 2007; Jiménez, Fabra, Talens, & Chiralt, 2012; Mali, Grossmann, García, Martino, & Zaritzky, 2002, 2006; Psomiadou, Arvanitoyannis, & Yamamoto, 1996). The development of entirely biodegradable polymers from agricultural resources has received considerable attention (García, Ribba, Dufresne, Aranguren, & Goyanes, 2011; Lu, Weng, & Cao, 2006; Mathew & Dufresne, 2002; Mathew, Thielemans, & Dufresne, 2008). Starch is probably the most promising renewable naturally biodegradable polymer since it is a versatile, cheap, and abundant biopolymer that does not itself have a fossil source (Savadekar & Mhaske, 2012). High-amylose starches possess more advantages than low-amylose ones and the films prepared from high-amylose starches have better mechanical strength and gas barrier properties (Lourdin, Della-Valle, & Colonna, 1995; Palviainen et al., 2001; Wolff, Davis, Cluskey, Gundrum, & Rist, 1951). Pea starches (PS) have a high amylose content, mostly ranging from 30 to 60%, varying with species (Hoover, Hughes, Chung, & Liu, 2010), and this makes them very useful in forming films (Palviainen et al., 2001).

However, like other hydrocolloids, starch films exhibit several drawbacks when compared to plastic polymers, such as their hydrophilic character and poor mechanical properties, which can be improved by blending with other compounds in the film (Briassoulis, 2004). Sun, Chu, Xiong, and Si (2013) reported that pea starch films blended with peanut protein isolate have better mechanical properties than pure pea starch film. Singha and Himanshu (2014) found that reinforcing films of blended starch and polyvinyl alcohol with silk fibroin could apparently improve their mechanical and water-resistance properties. Shi, Wang, Li, and Adhikari (2013) reported that water vapor permeability (WVP) of corn starch film is significantly higher than that of starch films containing spray dried and vacuum freeze dried starch nanoparticles.

Starch is a natural semicrystalline biopolymer which is biodegradable, renewable and abundant. Starch-based nanoparticles are widely used as drug carriers due to their non-toxicity, biocompatibility and biodegradability (Han, Gao, & Liu, 2013; Rajisha, Maria, Pothan, Ahmad, & Thomas, 2014). In recent years, nanowhiskers and nanocrystals have also been applied to reinforce biodegradable and non-biodegradable polymeric matrices (Lu, Weng, & Zhang, 2004; Samir, Alloin, Gorecki, Sanchez, & Dufresne, 2004). The diameter of starch nanocrystals (SNCs) prepared by sulfuric acid hydrolysis is about 20 nm, which results in many great achievements when compounded with polymer

* Corresponding author at: College of Food Science and Engineering, Qingdao Agricultural University, 266109, 700 Changcheng Road, Chengyang District, Qingdao, China. Tel.: +86 532 88030448; fax: +86 532 88030449.
E-mail address: phdsun@163.com (Q. Sun).

http://dx.doi.org/10.1016/j.carbpol.2014.12.040
0144-8617/

matrices. Chen, Cao, and Huneault (2008) reported the poly(vinyl alcohol)/pea starch nanocrystals nanocomposite films containing 5 and 10 wt% of nanocrystals content possessed improved physical properties than pure PVA film. Using a soy protein isolate (SPI) as a matrix, Zheng, Ai, Chang, Huang, and Dufresne (2009) reported an increase in strength and Young's modulus at pea starch nanocrystal loading levels lower than 2 wt%. Wang and Zhang (2008) described the preparation of high-strength water-borne polyurethane (WPU)-based elastomer reinforced with 1–5% waxy maize starch nanocrystals.

However, the preparation and characteristics of high-amylose starch-based films containing SNCs, to our knowledge, have not been reported so far. Therefore, this work investigates mechanical, barrier, and morphological properties of pea starch films reinforced with different amounts of SNCs to determine whether SNCs can improve the functional properties of pea starch films. This will provide the theoretical basis to produce biodegradable starch films that have better mechanical and barrier properties.

2. Materials and methods

2.1. Materials

Pea starch (about 40% amylose) was purchased from Tianjin Tingfung Starch Development Co., Ltd. (Tianjin, China). Waxy maize starch (98% amylopectin) was kindly provided by the same company. Glycerol was purchased from Sigma–Aldrich Co., Ltd. (St. Louis, MO., United States). Sulfuric acid (H_2SO_4), potassium carbonate (K_2CO_3) and other analytical grade reagents were purchased from Shanghai Sinopharm Chemical Reagent Co., Ltd. (Shanghai, China).

2.2. Preparation of SNCs

SNCs were prepared by acid hydrolysis of waxy maize starch according to the method of Angellier, Choisnard, and Molina-Boisseau (2004). Typically, 15% starch dispersion was prepared with a diluted sulfuric acid solution (3.16 M, 300 mL) and stirred constantly at 200 r/min with 40 °C water curing treatment for seven days. After hydrolysis, the suspensions were washed using successive centrifugations in distilled water until neutrality, then the precipitate was vacuum freeze-dried to obtain SNCs.

2.3. Preparation of PS/SNCs films

Following the method of Sun, Sun, and Xiong (2013), (5).0 g of pea starch and 1.5 g of glycerol plasticizer were added to 100 mL deionized water to form starch-plasticizer dispersions. Each dispersion was thoroughly stirred for 30 min in a thermostatic water bath at boiling temperature, and then cooled to 50 °C. Aliquots of SNCs (0, 0.05, 0.15, 0.25, 0.35 and 0.45 g respectively) were added to 50 mL deionized water, then treated by ultrasonic wave (KQ-400KDE, Kun-Shan Ultrasonic instrument Co., Ltd., Jiangsu, China) at 100 W for 10 min to ensure uniform dispersion. These SNCs dispersions were then added to the starch-plasticizer dispersions, stirring continuously for 30 min. After that, the film-forming dispersions were degassed, cast at 5.6 mg solids/cm^2 in a framed and leveled polytetrafluoroethylene plate having a diameter of 15 cm diameter) and dried at 40 °C overnight. The films were peeled from the casting plates and conditioned for at least one week at 43% relative humidity, conditioned by using a K_2CO_3 saturated solution.

2.4. Thickness of PS/SNCs films

The thickness of the films was determined using a digital micrometer (Vernier, China, 0.001 mm accuracy). Reported thickness values were the mean of ten measurements taken from each film sample. The average value for each film was used to calculate its tensile properties and water vapor permeability.

2.5. Opacity

The transparency of the films were determined by measuring their light absorption at wavelength of 600 nm, using a UV–visible spectrophotometer Shimadzu 1601 PC (Tokyo, Japan), according to the method described by Maran, Sivakumar, Sridhar, and Thirugnanasambandham (2013). The film specimens were cut into strips (1 cm × 4 cm) and placed directly in the spectrophotometer test cell. Air was used as reference. Opacity was expressed as absorbance units per thickness unit.

2.6. Color measurement

Sample surface color was analyzed with a colorimeter (CR-400 Minolta Chroma Meter; Konica Minolta Sensing Inc., Tokyo, Japan) according to the method described by Jang, Shin, and Song (2011) with some modifications. Samples (50 mm × 50 mm strips) were placed onto a white standard plate, and Hunter values (L^*, a^* and b^*) were measured. The Hunter L^*, a^*, and b^* values for the standard plate were $L^* = 96.68$, $a^* = 0.14$, and $b^* = 1.94$. For each sample, five measurements were taken at different locations.

2.7. Mechanical properties

A TA. XT Plus Texture Analyzer (Lloyd Instruments, West Sussex, England) was used to determine the film's tensile strength (TS), elongation at break (E%) and elastic modulus (M). Film specimens were tested as suggested by Mehyar, Al-Ismail, Han, and Chee (2012), with some modifications, and the tests were carried out according to the ASTM D828-97 standard test methods (ASTM, 1997). PS/SNCs composite films were cut into strips (1 cm × 10 cm). The strips were then preconditioned at 67% RH for 48 h inside a sealed desiccator containing saturated sodium chloride solution at room temperature (25 ± 1 °C). The films were loaded into the testing system, which was set at an initial sample length and grip speed of 2 cm and 100 mm/min, respectively. TS was calculated by dividing maximum load by the film's cross-sectional area. E% was expressed as the percentage of change in the original length of a specimen between the grips at break. M was the slop of the tensile stress–strain curve over the elastic (linear) region.

2.8. Measurement of the moisture content of PS/SNCs composite films

The moisture content of the films was determined using the gravimetric method (Carmen, Müllera, João, and Fabio, 2011). The weight of film samples (4 cm × 4 cm) was determined, then the samples were dried at 105 °C for 24 h, after which the weight of the dried samples was determined as well. The moisture content of PS/SNCs composite films is expressed in g water/g dry mass.

2.9. Measurement of water vapor permeability (WVP) and water-vapor transmission rate (WVTR)

The gravimetric method was used to determine the WVP and WVTR of the PS/SNCs composite films, as suggested by Latifa, Pfannstielb, and Makkara (2013) and the tests were carried out according to the ASTM E96-00 (ASTM, 2000) methodology. Circular film samples with a diameter of approximately 10 mm were placed over the mouth of the test cup and sealed using melted paraffin. The cup was prefilled with anhydrous calcium chloride leaving 3 mm

Table 1
Opacity and color parameters of PS/SNCs composite films.

Sample	Opacity	L^*	a^*	b^*
PS	2.23 ± 0.09^{c}	86.93 ± 0.15^{b}	1.15 ± 0.01^{a}	2.10 ± 0.02^{e}
PS + 1% SNCs	2.29 ± 0.11^{c}	86.71 ± 0.35^{b}	1.11 ± 0.01^{abc}	2.29 ± 0.03^{d}
PS + 3% SNCs	2.31 ± 0.06^{c}	87.39 ± 0.18^{a}	1.13 ± 0.04^{ab}	2.46 ± 0.09^{c}
PS + 5% SNCs	2.44 ± 0.13^{c}	86.81 ± 0.05^{b}	1.08 ± 0.03^{bc}	2.55 ± 0.17^{c}
PS + 7% SNCs	2.67 ± 0.16^{b}	87.33 ± 0.18^{a}	1.05 ± 0.03^{c}	3.22 ± 0.10^{b}
PS + 9% SNCs	2.93 ± 0.05^{a}	86.79 ± 0.28^{b}	1.07 ± 0.06^{bc}	4.01 ± 0.13^{a}

The values correspond to the mean ± standard deviation. Values within each column followed by different letters indicate significant differences ($p < 0.05$).
PS represents pea starch, SNCs represents waxy corn starch nanocrystals.

below the top. After the film specimens were equipped, the assembly was weighed and placed in a chamber conditioned at 25 °C and 100% RH. The cup's weight increments were measured and plotted at intervals. The slope of the straight line was calculated with a linear regression. The WVP was calculated as follows:

$$\mathrm{WVP} = \frac{m \times d}{A \times t \times P} \quad (1)$$

$$\mathrm{WVTR} = \frac{m}{A \times t} \quad (2)$$

where d is film thickness in meters, m is the weight increment of the cup (g), A is the area exposed (m^2), t is the time lag for permeation (h), and P is water vapor's partial pressure difference across the film (Pa). All specimens were tested three times.

2.10. Scanning electron microscopy (SEM)

The surfaces and cross-sections of the composite films were observed using a JSM-5610LV SEM (JEOL, Tokyo, Japan), according to the description of De la Caba et al. (2012). The films were frozen in liquid nitrogen, then vacuum freeze dried immediately. Prior to photographic observation, the fracture surfaces were sputter-coated with a layer of gold to avoid charging under the electron beam.

2.11. Differential scanning calorimetry (DSC)

DSC experiments were carried out by using DSC1 (METTLER TOLEDO, Switzerland). The calorimeter was calibrated with indium (melting point 156.6 °C, heat of fusion 28.5 J/g). The DSC runs were operated under nitrogen gas atmosphere (30 mL/min) and an empty pan was used as the reference. The film samples, approximately 3 mg, were hermetically sealed in aluminum pans. The pans were heated from 15 to 300 °C at the scanning rate of 10 °C/min. The DSC thermograms were evaluated to characterize the onset, peak and end temperatures and the enthalpy changes of the phase transitions (Sun, Xi, Li, & Xiong, 2014).

2.12. Thermogravimetric analysis (TG)

The thermogravimetric analysis (TGA) was performed with a Shimadzu model TGA-50TA for the PS films with and without SNCs. The films (4.0 ± 1.0 mg) were heated from 40 to 600 °C using a platinum crucible under air atmosphere with a flow rate of 20 mL/min. The heating rate was 5 °C/min.

2.13. Statistical analysis

All the data obtained were average values of triplicate determinations and subjected to statistical analysis using SPSS 17.0 (SPSS Inc., 160 Chicago, USA). The data were analyzed using analysis of variance (ANOVA) and expressed as mean values ± standard deviation. Differences were considered at a significant level of 95% ($p < 0.05$).

3. Results and discussion

3.1. Opacity and color parameters of PS/SNCs composite films

Table 1 shows the opacity and transparent values L^*, a^*, b^* of the PS films with and without SNCs. Contrast to control film, the composite films were less transparent since the opacity increased with increasing SNCs ratio in PS/SNCs composites. This could be ascribed to agglomeration of nanoparticles. Castillo et al. (2013) also reported that film opacity increased significantly with an increase in talc concentration in thermoplastic corn starch formulations, and reduced light transmittance of films. The higher opacity will improve the ability of the films to protect package contents from light and enhance the quality of the packaged food.

Color is a vital index of the films in terms of appearance and the consumer acceptance of packaged products. As shown in Table 1, there was little difference in the L^* and a^* value of the films with and without SNCs, which indicated that the effect of SNCs on the L^* and a^* value were not significant. However, the composite films showed higher values ($p < 0.05$) of b^* parameter (blue-yellow) compared to pure PS film, which meant that the composite became more yellow. Similarly, Nafchi and Alias (2013) founded that introducing the nanoclay resulted in yellowing of the sago starch films.

3.2. Mechanical properties of the films

The TS, E% and M of the PS/SNCs composite films are shown in Table 2. TS and M of the composite films increased, while the E% decreased compared to the pure PS film. The composite film

Table 2
Mechanical properties of PS/SNCs composite films.

Sample	Thickness (μm)	TS (MPa)	E (%)	M (MPa)
PS	104.0 ± 0.96^{f}	5.76 ± 0.02^{f}	29.23 ± 0.56^{a}	21.15 ± 0.25^{d}
PS + 1% SNCs	109.4 ± 0.78^{d}	6.56 ± 0.006^{e}	26.18 ± 0.82^{b}	27.95 ± 0.86^{c}
PS + 3% SNCs	106.8 ± 0.92^{e}	6.95 ± 0.04^{c}	20.46 ± 0.79^{c}	37.89 ± 0.17^{b}
PS + 5% SNCs	117.8 ± 0.49^{c}	9.96 ± 0.02^{a}	12.58 ± 0.66^{d}	85.72 ± 0.98^{a}
PS + 7% SNCs	121.0 ± 0.83^{b}	7.12 ± 0.01^{b}	21.6 ± 0.55^{c}	36.59 ± 1.02^{b}
PS + 9% SNCs	131.2 ± 0.49^{a}	6.68 ± 0.02^{d}	26.7 ± 0.49^{b}	27.56 ± 0.03^{c}

The values correspond to the mean ± standard deviation. Values within each column followed by different letters indicate significant differences ($p < 0.05$).
PS represents pea starch, SNCs represents waxy corn starch nanocrystals, TS represents tensile strength, E represents elongation at break, M represents elastic modulus.

Table 3
Water vapor permeability of PS/SNCs composite films.

Sample	Moisture (%)	WVP (g mm/m^2 h Pa)	WVTR (g/m^2 h)
PS	38.74 ± 1.89^a	11.18 ± 0.47^a	6.16 ± 0.06^a
PS + 1% SNCs	30.19 ± 0.86^b	7.57 ± 0.16^b	5.61 ± 0.02^b
PS + 3% SNCs	25.23 ± 0.75^c	6.09 ± 0.11^c	4.39 ± 0.06^c
PS + 5%SNCs	23.17 ± 0.66^d	4.26 ± 0.19^e	3.26 ± 0.01^e
PS + 7%SNCs	29.12 ± 0.93^b	5.41 ± 0.14^d	3.67 ± 0.03^d
PS + 9%SNCs	26.42 ± 0.98^c	5.50 ± 0.18^d	4.19 ± 0.66^c

The values correspond to the mean ± standard deviation. Values within each column followed by different letters indicate significant differences ($p < 0.05$).
PS represents pea starch, SNCs represents means waxy corn starch nanocrystals, WVP represents water vapor permeability; WVTR represents means water-vapor transmission rate.

with 5% additional SNCs had the highest TS of 9.96 MPa, a 72.9% increase over the control film. At the same time, the *E*% values decreased to 12.58% at the minimum. The reason for the enhancement of the composite film's mechanical properties may be the denser structure and greater stiffness of SNCs (LeCorre, Bras, & Dufresne, 2010). However, when the percentage of additional SNCs was 7–9%, the TS decreased while the *E*% values increased. This phenomenon was probably because of the large number of hydroxyl groups in the surface of the SNCs, which caused the SNCs to link together, leading to micro-phase separation, as proposed by García et al. (2011).

3.3. Water vapor barrier permeability of PS/SNCs composite films

Table 3 shows how the water vapor barrier permeability properties of PS/SNCs composite films varied according to different SNCs contents. The percentage of moisture, WVP and WVTR of PS/SNCs composite films significantly decreased with the addition of SNCs. When the level of SNCs was 5%, the WVP of the films was lowest, clearly indicating that the water barrier properties of the composite films were improved. A likely reason was because SNCs dispersed easily throughout the matrix of starch and made the films more compact (Shi et al., 2013). The presence of such filler concentrations probably constituted a tortuous path for water molecules to pass through. A longer diffusive path for water molecules reduces permeability (Sihna & Okamoto, 2003). However, as SNCs were added, especially above the 5% threshold, the water resistance of the composite film decreased, possibly because of the aggregation of SNCs failed to prevent the migration of water molecules effectively (Muller, Laurindo, & Yamashita, 2011; Rhim, Lee, & Kwak, 2005).

3.4. SEM images of the surface of PS/SNCs composite films

Fig. 1 shows the surface morphology of the composite films with different amounts of SNCs. The surface of the control film was smooth and compact, while the films became rougher as the SNCs content increased. SNCs dispersed homogeneously in the PS/SNCs composite films at concentrations of 1–5%. At exactly 5% SNCs content, the surface of the PS/SNCs composite films remained relatively smooth and compact without any aggregation of SNCs, which were consistent with observed properties. However, with 7% or more SNCs addition, the SNCs aggregated in the composite films, and many nanowires of 2–30 μm length and about 200 nm diameter could be observed (Fig. 1). The formation of nanowires in the films was very interesting and probably contributed to the self-assembly of SNCs or their interaction with the amylose of the pea starch, phenomena which need further investigation. Similarly, Duan, Sun, Wang, and Yang (2011) found that SNCs dispersed well in chitosan films with no obvious aggregation when the SNCs content was lower than 30%, but beyond this point, the SNCs aggregated, which resulted in rougher composite films. Avik, Ruhul, and Stephane (2012) reported that the chitosan films showed homogeneous and smooth structure with the addition of 5% cellulose nanocrystals (NCCs). However, the surface became rougher with the increase of NCC. When the NCC contents grew beyond 10%, white holes appeared on the surface of films.

3.5. SEM image of the cross-section of PS/SNCs composite films

Fig. 2 shows the morphology and structure of the cross-section of the PS/SNCs composite films. There were obvious longitudinal ripples under the cross-section of the control films. These became transverse ripples with the addition of SNCs. The PS/SNCs composite films' transverse fibrous structure in their cross-sections was most apparent when the level of additional SNCs was 1%, though further cracks appeared as SNCs content increased. However, with the addition of 5% SNCs, the structure of the composite film's cross-section became denser and lacked obvious cracks, possibly because the hydroxyl group on the SNCs' surface interacted with the hydroxyl group on the pea starch's surface. Similarly, the gel network structure formed through the hydrogen bonds when the hydroxyl group of the SNCs combined with that of pea starch (Yao, Cai, and Tang, 2011). However, when 7% or more SNCs was added to the pea films, cracks appeared in the structure of composite films because of the aggregation of SNCs arising from their intermolecular interactions (Chang, Ai, Chen, Dufresne, & Huang, 2009).

3.6. Thermal properties of PS/SNCs composite films

As shown in Table 4, compared to pure PS film, a higher melting temperature (T_m) of the composite films with 5% SNCs could be observed, which may be attributed to the strong interactions between SNCs and films. Suárez et al. (2013) also reported the increase in the T_m of composite films with cellulose nanoparticles. The addition of SNCs (lower than 5%) increased the enthalpy value of the composite films. This may be due to the interactions between SNCs and chain segments of PS, which increased the crystallinity of the film. It could be deduced that the higher values of the melting enthalpy, the higher compatibility of PS and SNCs. However, when the concentration of SNCs was more than 5%, the melting enthalpy values of composite films decreased. That could be because higher filler concentration hindered lateral rearrangements of starch chains and crystallization of starch films (Kaushik, Singh, & Verma, 2010).

3.7. The thermal stability of PS/SNCs composite films

The thermal stability of composite films was characterized using thermogravimetric analysis. Fig. 3 showed an initial drop between 50 and 150 °C, which resulted from the loss of water. Teixeira et al. (2009) reported that the mass loss from 100 °C to the onset decomposition temperature was related to the evaporation of water. The

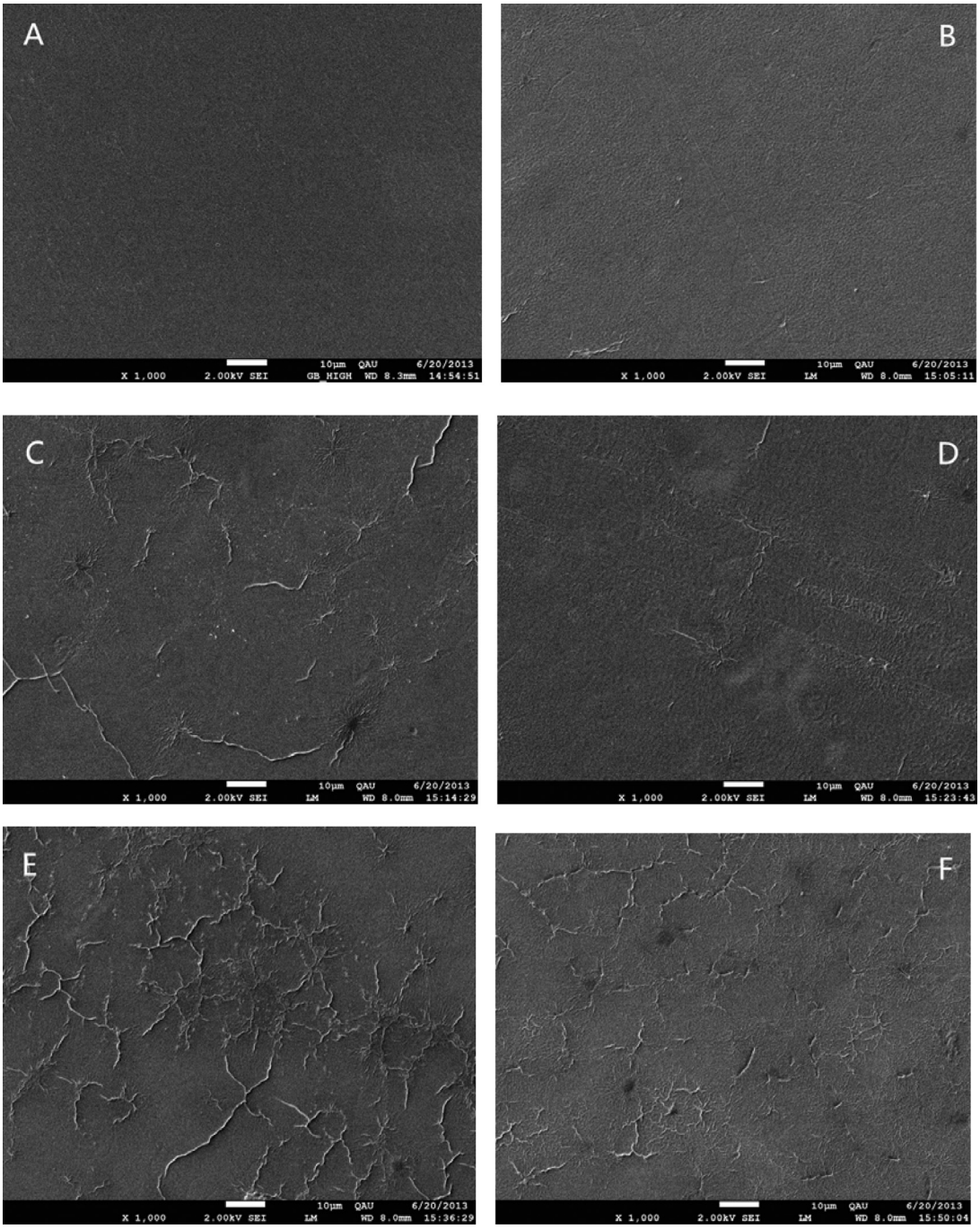

Fig. 1. SEM images of the surface of PS/SNCs composite films.

Table 4
Thermal properties of PS/SNC blending film.

Sample	T_o (°C)	T_m (°C)	T_c (°C)	ΔH (J/g)
PS	186.61 ± 1.31^{a}	188.51 ± 0.55^{b}	196.77 ± 3.11^{b}	23.51 ± 0.21^{c}
PS + 1%SNC	186.26 ± 2.54^{a}	190.81 ± 4.11^{ab}	196.19 ± 0.66^{b}	24.34 ± 0.05^{b}
PS + 3%SNC	186.79 ± 0.93^{a}	189.56 ± 2.39^{b}	196.95 ± 1.79^{b}	24.75 ± 0.32^{b}
PS + 5%SNC	187.35 ± 3.55^{a}	193.92 ± 0.78^{a}	199.47 ± 2.12^{a}	26.76 ± 1.09^{a}
PS + 7%SNC	186.61 ± 2.12^{a}	189.66 ± 1.80^{b}	198.32 ± 3.15^{ab}	22.31 ± 0.66^{d}
PS + 9%SNC	187.54 ± 1.96^{a}	190.10 ± 3.94^{ab}	199.84 ± 0.27^{a}	22.17 ± 0.25^{d}

The values correspond to the mean ± standard deviation. Values within each column followed by different letters indicate significant differences ($p < 0.05$).
PS represents pea starch, SNCs represents waxy corn starch nanocrystals, T_o represents onset temperature, T_m represents melting temperature, T_c represents endset temperature, ΔH represents enthalpy of gelatinization.

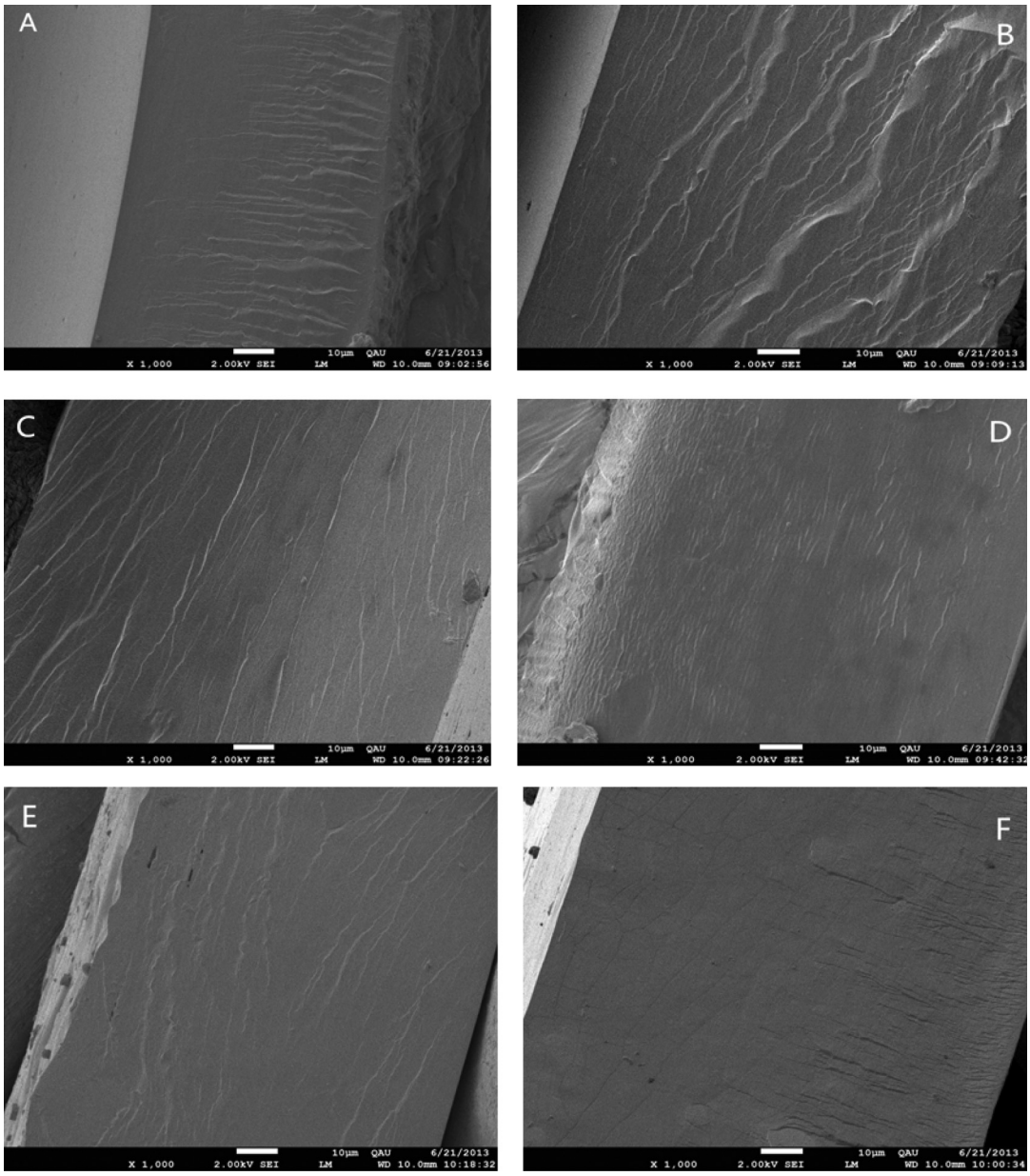

Fig. 2. SEM images of the cross section of PS/SNCs composite films.

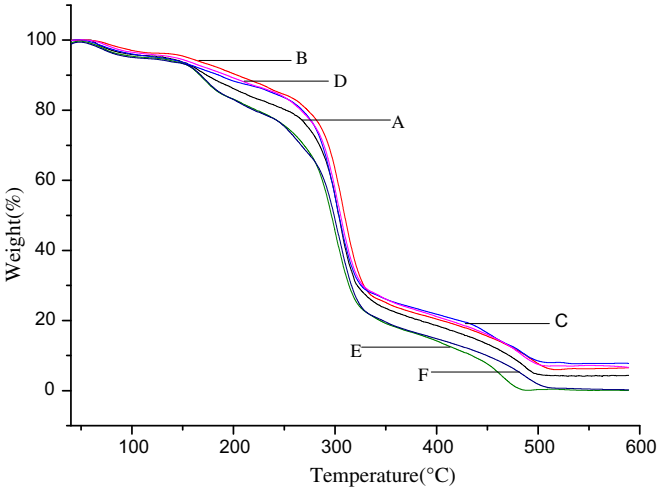

Fig. 3. Thermogravimetric curves of PS/SNCs composite films.

main mass loss took place between 250 and 330 °C, which was ascribed to the decomposition of polymeric films. The films adding 1, 3 and 5% SNCs showed higher thermal decomposition temperature than pure starch film, which gave evidence that the addition of suitable amount of SNCs could improve the thermal stability of starch films. However, the composite films with more than 5% SNCs had worse thermal stability, even worse than pure starch films. This was attributed to the presence of lots of sulfate groups at the surface of SNCs (Angellier, Molina-Boisseau, Lebrun, & Dufresne, 2005; LeCorre, Bras, & Dufresne, 2012) which catalyzed the depolymerization of SNCs.

4. Conclusion

Waxy maize starch nanocrystals (SNCs)-reinforced pea starch films showed better mechanical, water vapor barrier and morphological properties than pure pea starch film. Increasing SNCs content (less than 5%) improved the measured values of tensile strength and elastic modulus in the nanocomposite films.

The moisture content, water vapor permeability, and water-vapor transmission rate of the films significantly decreased with the increase of SNCs content, the thermal stability was significantly improved (not more than 5%). The nanocomposites with 5% SNCs presented smooth surface and dense cross-section observed by SEM. Thus, this study demonstrates the potential of SNCs-reinforced pea starch films for developing environmentally friendly and energy saving packaging materials.

Acknowledgment

Financial support from the Qingdao Municipal Science and Technology Plan Project (14-2-3-48-nsh) is gratefully acknowledged.

References

Angellier, H., Choisnard, L., & Molina-Boisseau, S. (2004). Optimization of the preparation of aqueous suspensions of waxy maize starch nanocrystals using a response surface methodology. *Biomacromolecules*, *5*, 1545–1551.

Angellier, H., Molina-Boisseau, S., Lebrun, L., & Dufresne, A. (2005). Processing and structural properties of waxy maize starch nanocrystals reinforced natural rubber. *Macromolecules*, *38*(9), 3783–3792.

ASTM D 882. (1997). Standard test method for tensile properties of thin plastic sheeting. In *Annual book of ASTM standards*. American Society for Testing and Materials.

ASTM E 96. (2000). Standard method for water vapor transmission of materials. In *Annual book of ASTM standards*. American Society for Testing and Materials.

Avik, K., Ruhul, A. K., & Stephane, S. (2012). Mechanical and barrier properties of nanocrystalline cellulose reinforced chitosan based nanocomposite films. *Carbohydrate Polymers*, *90*, 1601–1608.

Briassoulis, D. (2004). An overview on the mechanical behavior of biodegradable agricultural films. *Journal of Polymers and the Environment*, *12*, 65–81.

Carmen, M. O., Müllera, B., João, B. L., & Fabio, Y. (2011). Effect of nanoclay incorporation method on mechanical and water vapor barrier properties of starch-based films. *Industrial Crops and Products*, *33*, 605–610.

Castillo, L., López, O., López, C., Zaritzky, N., García, M. A., Barbosa, S., et al. (2013). Thermoplastic starch films reinforced with talc nanoparticles. *Carbohydrate Polymers*, *95*, 664–674.

Chang, P. R., Ai, F., Chen, Y., Dufresne, A., & Huang, J. (2009). Effects of starch nanocrystal graft polycaprolactone on mechanical properties of waterborne polyurethane-based nanocomposites. *Journal of Applied Polymer Science*, *111*, 619–627.

Chen, Y., Cao, X. D., Peter, R. C., & Michel, A. H. (2008). Comparative study on the films of poly (vinyl alcohol)/pea starch nanocrystals and poly (vinyl alcohol)/native pea starch. *Carbohydrate Polymers*, *73*, 8–17.

De la Caba, K., Pena, C., Ciannamea, E. M., Stefani, P. M., Mondragon, I., & Ruseckaite, R. A. (2012). Characterization of soybean protein concentrate-stearic acid/palmitic acid blend edible films. *Journal of Applied Polymer Science*, *124*, 1796–1807.

Duan, B., Sun, P. D., Wang, X. L., & Yang, C. (2011). Preparation and properties of starch nanocrystals/carboxymethyl chitosan nanocomposite films. *Starch/Stärke*, *63*, 528–535.

Famá, L., Goyanes, S., & Gerschenson, L. (2007). Influence of storage time at room temperature on the physicochemical properties of cassava starch films. *Carbohydrate Polymers*, *70*, 265–273.

García, N. L., Ribba, L., Dufresne, A., Aranguren, M., & Goyanes, S. (2011). Effect of glycerol on the morphology of nanocomposites made from thermoplastic starch and starch nanocrystals. *Carbohydrate Polymers*, *84*, 203–210.

Hoover, R., Hughes, T., Chung, H. J., & Liu, Q. (2010). Composition, molecular structure, properties, and modification of pulse starches: a review. *Food Research International*, *43*, 399–413.

Han, F., Gao, C. M., & Liu, M. Z. (2013). Fabrication and characterization of size-controlled starch-based nanoparticles as hydrophobic drug carriers. *Journal of Nanoscience and Nanotechnology*, *13*, 6996–7007.

Jang, S. A., Shin, Y. J., & Song, K. B. (2011). Effect of rapeseed protein–gelatin film containing grapefruit seed extract on 'Maehyang' strawberry quality. *International Journal of Food Science and Technology*, *46*, 620–625.

Jiménez, A., Fabra, M. J., Talens, P., & Chiralt, A. (2012). Effect of recrystallization on tensile, optical and water vapour barrier properties of corn starch films containing fatty acids. *Food Hydrocolloids*, *26*(1), 302–310.

Kaushik, A., Singh, M., & Verma, G. (2010). Green nanocomposites based on thermoplastic starch and steam exploded cellulose nanofibrils from wheat straw. *Carbohydrate Polymer*, *82*, 337–345.

Latifa, S. J., Pfannstielb, H. P. S., & Makkara, K. B. (2013). Amino acid composition, antinutrients and allergens in the peanut protein fraction obtained by an aqueous enzymatic process. *Food Chemistry*, *136*, 213–217.

LeCorre, D., Bras, J., & Dufresne, A. (2010). Starch nanoparticles: A review. *Biomacromolecules*, *11*, 1139–1153.

LeCorre, D., Bras, J., & Dufresne, A. (2012). Influence of native starch's properties on starch nanocrystals thermal properties. *Carbohydrate Polymers*, *87*(1), 658–666.

Lourdin, D., Della-Valle, G., & Colonna, P. (1995). Influence of amylase content of starch films and foams. *Carbohydrate Polymers*, *27*, 261–270.

Lu, Y. S., Weng, L. H., & Zhang, L. N. (2004). Morphology and properties of soy protein isolate thermoplastics reinforced with chitin whiskers. *Biomacromolecules*, *5*, 1046–1051.

Lu, Y., Weng, L., & Cao, X. (2006). Morphological, thermal and mechanical properties of ramie crystallites-reinforced plasticized starch biocomposites. *Carbohydrate Polymers*, *63*, 198–204.

Mali, S., Grossmann, M. V. E., García, M. A., Martino, M. N., & Zaritzky, N. E. (2002). Microstructural characterization of yam starch films. *Carbohydrate Polymers*, *50*, 379–386.

Mali, S., Grossman, M. V. E., García, M. A., Martino, M. N., & Zaritzky, N. E. (2006). Effects of controlled storage on thermal, mechanical and barrier properties of plasticized films from different starch sources. *Journal of Food Engineering*, *75*, 453–460.

Maran, J. P., Sivakumar, V., Sridhar, R., & Thirugnanasambandham, K. (2013). Development of model for barrier and optical properties of tapioca starch based edible films. *Carbohydrate Polymers*, *92*, 1335–1347.

Mathew, A. P., & Dufresne, A. (2002). Morphological investigation of nanocomposites from sorbitol plasticized starch and tunicin whiskers. *Biomacromolecules*, *3*, 609–617.

Mathew, A. P., Thielemans, W., & Dufresne, A. (2008). Mechanical properties of nanocomposites from sorbitol plasticized starch and tunicin whiskers. *Journal of Applied Polymer Science*, *109*, 4065–4074.

Mehyar, G. F., Al-Ismail, K., Han, J. H., & Chee, G. W. (2012). Characterization of edible coatings consisting of pea starch, whey protein isolate, and carnauba wax and their effects on oil rancidity and sensory properties of walnuts and pine nuts. *Journal of Food Science*, *77*, 52–59.

Muller, C. M. O., Laurindo, J. B., & Yamashita, F. (2011). Effect of nanoclay incorporation method on mechanical and water vapor barrier properties of starch-based film. *Industrial Crops and Products*, *33*, 605–610.

Nafchi, M. A., & Alias, A. K. (2013). Mechanical, barrier, physicochemical, and heat seal properties of starch films filled with nanoparticles. *Journal of Nano Research*, *25*, 90–100.

Palviainen, P., Heinamaki, J., Myllarinen, P., Lahtinen, R., Yliruusi, J., & Forsseell, P. (2001). Corn starches as film formers in aqueous based film coating. *Pharmaceutical Development and Technology*, *6*, 353–361.

Psomiadou, E., Arvanitoyannis, I., & Yamamoto, N. (1996). Edible films made from natural resources; microcrystalline cellulose (MCC), methylcellulose (MC) and corn starch and polyols Part 2. *Carbohydrate Polymers*, *31*, 193–204.

Rajisha, K. R., Maria, H. J., Pothan, L. A., Ahmad, Z., & Thomas, S. (2014). Preparation and characterization of potato starch nanocrystal reinforced natural rubber nanocomposites. *International Journal of Biological Macromolecules*, *67*, 147–153.

Rhim, J. W., Lee, J. H., & Kwak, H. S. (2005). Mechanical and water barrier properties of soy protein and clay mineral composite. *Food Science and Biotechnology*, *14*, 112–116.

Samir, A., Alloin, F., Gorecki, W., Sanchez, J., & Dufresne, Alain. (2004). Nanocomposite polymer electrolytes based on poly(oxyethylene) and cellulose nanocrystals. *Journal of Physical Chemistry B*, *108*, 10845–10852.

Savadekar, N. R., & Mhaske, S. T. (2012). Synthesis of nano cellulose fibers and effect on thermoplastics starch based films. *Carbohydrate Polymers*, *89*, 146–151.

Shi, A. M., Wang, L. J., Li, D., & Adhikari, B. (2013). Characterization of starch films containing starch nanoparticles Part 1: Physical and mechanical properties. *Carbohydrate Polymers*, *96*, 593–601.

Sihna, R. S., & Okamoto, M. (2003). Polymer/layered silicate nanocomposites: a review from preparation to processing. *Progress in Polymer Science*, *28*, 1539–1641.

Singha, A. S., & Himanshu, K. (2014). Effect of silk fibroin reinforcement on the properties of potato starch-polyvinyl alcohol blend films. *International Journal of Polymer Analysis and Characterization*, *19*, 212–221.

Suárez, S. A., Rodríguez, H. M., Hernández, A. R., Hernández-Uribe, J. P., Bello-Pérez, L. A., & Vargas-Torres, A. (2013). Characterization of films made with chayote tuber and potato starches blending with cellulose nanoparticles. *Carbohydrates Polymers*, *98*, 102–107.

Sun, Q. J., Chu, L. J., Xiong, L., & Si, F. M. (2013). Effects of different isolation methods on the physicochemical properties of pea starch and textural properties of vermicelli. *Journal of Food Science and Technology*, *50*, 569–577.

Sun, Q. J., Sun, C. X., & Xiong, L. (2013). Mechanical, barrier and morphological properties of pea starch and peanut protein isolate blend films. *Carbohydrates Polymers*, *98*, 630–637.

Sun, Q. J., Xi, T. T., Li, Y., & Xiong, L. (2014). Characterization of corn starch films reinforced with $CaCO_3$ nanoparticles. *PLOS ONE*, *9*, e106727.

Teixeira, E. M., Pasquini, D., Curvelo, A. A. S., Corradini, E., Belgacem, M. N., & Dufresne, A. (2009). Cassava bagasse cellulose nanofibrils reinforced thermoplastic cassava starch. *Carbohydrates Polymers*, *78*, 422–431.

Wang, Y., & Zhang, L. (2008). High-strength waterborne polyurethane reinforced with waxy maize starch nanocrystals. *Journal of Nanoscience and Nanotechnology*, *8*, 5831–5838.

Wolff, I. A., Davis, H. A., Cluskey, J. E., Gundrum, L. J., & Rist, C. E. (1951). Preparation of films from amylose. *Industrial and Engineering Chemistry*, *43*, 915–919.
Yao, K. H., Cai, J., & Tang, S. W. (2011). Structure and properties of starch/PVA/nano-SiO_2 hybrid films. *Carbohydrate Polymers*, *86*, 1784–1789.
Zheng, H., Ai, F., Chang, P. R., Huang, J., & Dufresne, A. (2009). Structure and properties of starch nanocrystal reinforced soy protein plastics. *Polymer Composites*, *30*, 474–480.